Jinst

PUBLISHED BY IOP PUBLISHING FOR SISSA

RECEIVED: *April 6, 2009*
ACCEPTED: *June 4, 2009*
PUBLISHED: *July 9, 2009*

4th INTERNATIONAL CONFERENCE ON IMAGING TECHNOLOGIES IN BIOMEDICAL SCIENCES,
FROM MEDICAL IMAGES TO CLINICAL INFORMATION - BRIDGING THE GAP,
22–28 SEPTEMBER 2007,
MILOS ISLAND, GREECE

Integrating multiscale polar active contours and region growing for microcalcifications segmentation in mammography

N.S. Arikidis,[a] A. Karahaliou,[a] S. Skiadopoulos,[a] E. Likaki,[b] G. Panagiotakis[a] and L. Costaridou[a,1]

[a] *University of Patras, Department of Medical Physics, Faculty of Medicine, University of Patras, 265 00, Patras, Greece*
[b] *University of Patras, Department of Radiology, Faculty of Medicine, University of Patras, 265 00, Patras, Greece*

E-mail: Costarid@upatras.gr

ABSTRACT: Morphology of individual microcalcifications is an important clinical factor in microcalcification clusters diagnosis. Accurate segmentation remains a difficult task due to microcalcifications small size, low contrast, fuzzy nature and low distinguishability from surrounding tissue. A novel application of active rays (polar transformed active contours) on B-spline wavelet representation is employed, to provide initial estimates of microcalcification boundary. Then, a region growing method is used with pixel aggregation constrained by the microcalcification boundary estimates, to obtain the final microcalcification boundary. The method was tested on dataset of 49 microcalcification clusters (30 benign, 19 malignant), originating from the DDSM database. An observer study was conducted to evaluate segmentation accuracy of the proposed method, on a 5-point rating scale (from 5:excellent to 1:very poor). The average accuracy rating was 3.98 ± 0.81 when multiscale active rays were combined to region growing and 2.93 ± 0.92 when combined to linear polynomial fitting, while the difference in rating of segmentation accuracy was statistically significant ($p < 0.05$).

KEYWORDS: Medical-image reconstruction methods and algorithms, computer-aided so; X-ray mammography and scinto- and MRI-mammography

[1] Corresponding author.

doi:10.1088/1748-0221/4/07/P07009

Contents

1 Introduction

Mammography is one of the most reliable methods for early detection of breast carcinomas. However, it is difficult for radiologists to provide both accurate and uniform evaluation for the enormous number of mammograms generated in widespread screening. Morphology is an important clinical factor in microcalcifications diagnosis [1]. The success of morphology quantification from individual microcalcifications heavily depends upon the accuracy of the segmentation algorithm [2]. Segmentation and consequently automated interpretation remains a difficult task in the computer-aided diagnosis of microcalcifications due to microcalcifications's fuzzy nature, low contrast and low distinguishing ability from their surroundings [3].

A variety of segmentation methods have been reported either for computer aided detection or diagnosis schemes. However, recent comparative studies demonstrated the radial gradient-based methods to be convenient for microcalcification segmentation. Specifically, Paquerault et al. [4] proposed a radial gradient-based segmentation method, outperforming a region-growing and a watershed-based method. Bankman et al. [5] compared multitolerance region growing, active contours and a radial gradient-based algorithm with the last two methods performing equally, except that active contours were time consuming. The capability of active contours to directly generate closed parametric contours from images, along with the incorporation of a smoothness constraint, constitutes them as less sensitive to noise and spurious edges.

A novel application of polar active contours (active rays) on B-spline wavelet representation is combined with a region-growing algorithm for microcalcification segmentation. The accuracy of the proposed segmentation method was evaluated by means of an observer study.

2009 JINST 4 P07009

2 Materials and methods

2.1 Case sample

A pilot case sample was analyzed consisting of 49 biopsy proven microcalcification clusters (19 malignant and 30 benign) originating from 49 mammograms of 49 patients. All mammograms were selected from the Digital Database for Screening Mammography (DDSM), digitized with a LUMISYS laser scanner at a pixel size of 50 μm, downsampled to 100 μm, and 12-bits greyscale. For each cluster, the DDSM database provides information concerning subtlety, calcification morphology and assessment of malignancy following ACR BIRADS^{TM} specifications.

2.2 B-spline active contour

Active contours are widely used for segmentation purposes [6–9]. The main advantage of active contours is to detect edges that correspond to boundaries. This is accomplished by incorporating smoothness constraints that provide robustness to noise and spurious edges. A limitation is considered the weighting parameter for the smoothness constraints. In the multiscale representation of B-spline active contours the smoothness is implicitly build into the model, reducing the number of parameters associated with smoothness constraints [10].

An active contour $C(s)$ is a parametric function defined in the (x,y) image plane of an image $f(x,y)$. The equilibrium state of the active contour prerequisites the minimization of the contour's energy E_c. In the multiscale representation of B-spline active contours, the energy of the contour associated with the smoothness constraints is omitted. Thus, the contour's energy $E_{c,j}$ is computed at level j from the potential function P_j, which is monotonically decreasing toward the edges.

$$E_{C,j} = \int_c P_j\left(\mathrm{C}\left(s\right)\right)ds \tag{2.1}$$

Using a coarse-to-fine iteration strategy, contour's energy $E_{c,j}$ is minimized sequentially across scales. Initially, contour's energy $E_{c,j}$ is minimized at the coarsest scale. Upon convergence, the solution is propagated to the next finer scale where it is used as starting condition. The solution at the finest scale provides the boundary estimates [10].

2.3 Active rays on B-spline wavelet representation

In this study, active rays in B-spline wavelet representation were employed to obtain microcalcification boundary estimates at specific orientations. The most important aspect of active rays is the reduction of the contour point search from the 2D image plane to a 1D signal, thus considerably reducing computation time. Additionally, the initial model required in active contours was replaced in active rays by a seed pixel within the structure [11].

The proposed method was initialized by centering a region of interest (ROI) at the microcalcification, annotated by a seed pixel on the original image by an experienced radiologist. The B-spline representation of each ROI was generated at three levels *(j=0,1,2)* from Mallat's redundant dyadic wavelet transform [12]. The smoothing function (b^3) is a cubic B-spline and the wavelet filter is the Laplacian operator of the 2nd order derivative, widely used in microcalcification detection and segmentation [13, 14]. The wavelet coefficients $w_j(x,y)$were calculated as follows:

$$w_j\left(x,y\right) = \left|\nabla^2\left(b^3_{2^j} * f\right)\left(x,y\right)\right| \tag{2.2}$$

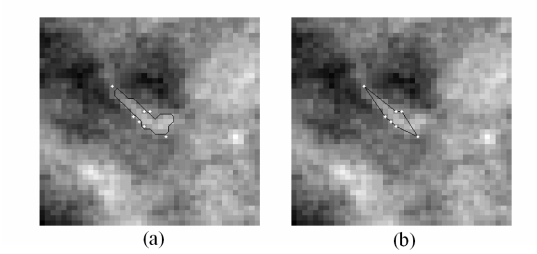

Figure 1. Magnified microcalcification delineated by (a) region growing constrained from boundary estimates, (b) linear polynomial fitting to boundary estimates.

Defining a reference point $m = (x_m, y_m)$ that lies within the microcalcification, an active ray $\rho_{m,j}(r,\theta)$ at a given orientation θ and radius r is defined at level j from wavelet coefficients w_j as:

$$\rho_{m,j}(r,\theta) = w_j(x_m + \mathrm{r}\cos(\theta), y_m + \mathrm{r}\sin(\theta)) \tag{2.3}$$

The contour's energy $E_{c,j}$ at polar coordinates (r,θ) and level j was defined as:

$$E_{C,j} = \int_0^{2\pi} P_j(r,\theta) d\theta \tag{2.4}$$

The potential P_j was defined at level j by the following monotonically decreasing function toward edges:

$$P_j(r,\theta) = \frac{\rho_{m,j}(\mathrm{r},\theta)}{r} \tag{2.5}$$

The denominator is a weighted term to ensure that small contours are not preferred over large contours [15]. Initially, the reference point is computed by a greedy algorithm as the closest local maximum to the seed pixel at dyadic scale 2^2. Then, the contour's energy $E_{c,j}$ was minimized at 8 orientations $(\theta = 0, \pi/4, 2\pi/4, \ldots, 7\pi/4)$ providing 8 microcalcification boundary estimates. At the finer dyadic scale (2^1) the reference point was repositioned at the closest local maximum. The microcalcification boundary estimates were repositioned proportionally to the reference point and refined by minimizing the contour's energy at corresponding orientations. The iteration algorithm does not propagate at dyadic scale 2^0 because this scale is mostly noise contaminated.

2.4 Active rays on B-spline wavelet representation

Gradient-based and region based methods are likely to perform better than either of the methods independently, being able to combine the complementary strengths of each individual method [16, 17].

In this study, microcalcification segmentation was achieved by region growing constrained from the boundary estimates, previously defined. Specifically, pixel aggregation was terminated by minimizing the least square error between the boundary estimates and the outermost pixels of the homogenous region at the same orientations. The method was compared with segmentation provided by linear polynomial fitting to the boundary estimates. Application examples of the two approaches are depicted in figure 1.

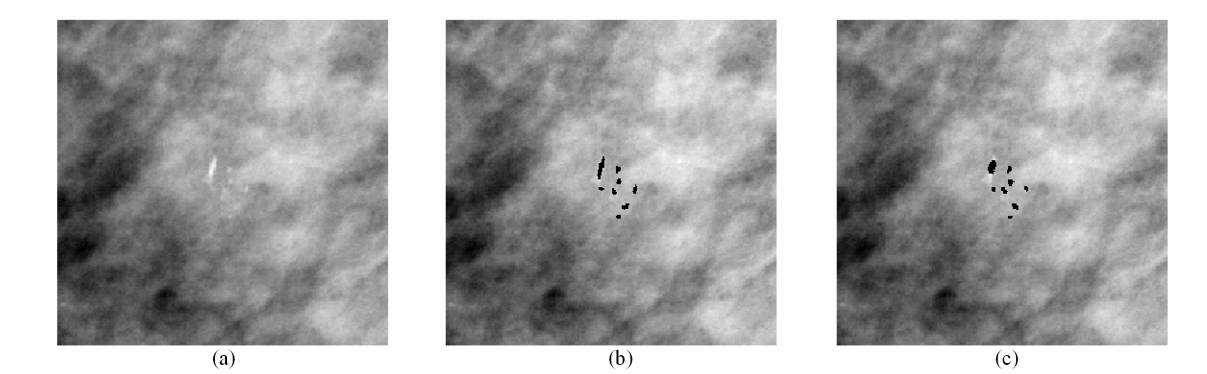

Figure 2. (a) Malignant microcalcification cluster (DDSM mammogram: C_0078_1.LEFT_CC). (b) Multiscale active rays with region growing. (c) Multiscale active rays with linear polynomial fitting.

3 Results and discussion

Figure 2 is an application example of multiscale active rays on a malignant microcalcification cluster, when combined with region growing (figure 2b) and when combined with linear polynomial fitting (figure 2c). As observed, both delineation methods have segmented accurately microcalcifications of small size and round shape. However, elongated and concave microcalcifications have been segmented more accurately by the region growing delineation.

An observer study was conducted to evaluate segmentation accuracy of the proposed method (multiscale active rays integrated with the region growing) and to compare it with multiscale active rays integrated with the linear polynomial fitting. The two segmentations of each microcalcification cluster were provided simultaneously in two softcopy display monitors (EIZO FlexScan L985EX 21.3"). An experienced radiologist was asked to evaluate segmentation accuracy of each method utilizing a 5-point accuracy rating. A microcalcification cluster was characterized with excellent accuracy when all individual microcalcifications were segmented precisely. The average and standard deviation of the radiologist's accuracy ratings were estimated for each segmentation method. The average rating of segmentation accuracy was 3.98 ± 0.81 when multiscale active contour were combined with region growing and 2.93 ± 0.92 when multiscale active rays were combined with linear polynomial fitting. This difference in average rating of segmentation accuracy was statistically significant (Wilcoxon signed ranks test, $p<0.05$).

4 Conclusion

An accurate algorithm is proposed for segmenting microcalcifications, integrating region and boundary information. Combination of multiscale active rays with region growing achieved a high accuracy rating, suggesting that the method fulfills human visual criteria. These results were attributed to the method's efficiency in segmenting microcalcifications of various sizes and more complex shapes. Active rays applied on B-spline multiscale representation allow fast computations while reducing the number of free parameters.

2009 JINST 4 P07009

Acknowledgments

This work was supported by the Karatheodory Programme (C.183) of the University of Patras, Greece.

References

[1] W.A. Berg et al., *Diagnostic imaging breast*, AMIRSYS, Canada (2006).

[2] W.J. Veldkamp and N. Karssemeijer, *Accurate segmentation and contrast measurement of microcalcifications in mammograms: A phantom study*, *Med. Phys.* **25** (1998) 1102.

[3] H.D. Cheng et al., *Computer-aided detection and classification of microcalcifications in mammograms: a survey*, *Pattern Recogn.* **36** (2003) 2967.

[4] S. Paquerault et al., *Radial gradient-based segmentation of mammographic microcalcifications: observer evaluation and effect on CAD performance*, *Med. Phys.* **31** (2004) 2648.

[5] I.N. Bankman et al., *Segmentation algorithms for detecting microcalcifications in mammograms*, *IEEE T. Inf. Technol. B.* **1** (1997) 141.

[6] M. Kass, A. Witkin and D. Terzopoulos, *Snakes: active contour models*, *Int. J. Comput. Vision* **1** (1988) 321.

[7] V. Caselles, R. Kimmel and G. Sapiro, *Geodesic active contours*, *Int. J. Comput. Vision* **22** (1997) 61.

[8] C. Xu and J.L. Prince, *Snakes, shapes, and gradient vector flow*, *IEEE T. Image Process.* **7** (1998) 359.

[9] J. Tang and S.T. Acton, *Vessel boundary tracking for intravital microscopy via multiscale gradient vector flow snakes*, *IEEE T. Bio.-Med. Eng.* **51** (2004) 316.

[10] P. Brigger, J. Hoeg and M. Unser, *B-spline snakes: a flexible tool for parametric contour detection*, *IEEE T. Image Process.* **9** (2000) 1484.

[11] J. Denzler and H. Niemann, *Active rays: polar-transformed active contours for real-time contour tracking*, *Real-Time Imaging* **5** (1999) 203.

[12] S. Mallat and S. Zhong, *Characterization of signals from multiscale edges*, *IEEE T. Pattern Anal.* **14** (1992) 710.

[13] A.F. Laine, S. Schuler, J. Fan and W. Huda, *Mammographic feature enhancement by multiscale analysis*, *IEEE T. Med. Imaging* **13** (1994) 725.

[14] R.N. Strickland and H.I. Hahn, *Wavelet transforms for detecting microcalcifications in mammograms*, *IEEE T. Med. Imaging* **15** (1996) 218.

[15] B. Appleton and H. Talbot, *Globally optimal geodesic active contours*, *J. Math. Imaging Vis.* **23** (2005) 67.

[16] T. Pavlidis and Y.T. Liow, *Integrating region growing and edge detection*, *IEEE T. Pattern Anal.* **12** (1990) 225.

[17] A. Chakraborty, A. Staib, and J.S. Duncan, *Deformable boundary finding in medical images by integrating gradient and region information*, *IEEE T. Med. Imaging* **15** (1996) 859.

2009 JINST 4 P07009